1 Interstellar magnetic fields

In this lecture I will cover some of the physical processes that are central to studies of magnetic fields in the interstellar medium (ISM), and the related techniques developed and used for their characterization. The field of research centred on this topic have significantly evolved in recent years and, as a consequence, not all techniques can be covered in a single lecture; we will therefore focus on a few from the more commonly used.

1.1 The Stokes parameters

Most (but not all) studies of interstellar magnetic fields involve the measurements of polarization either in spectral lines or in continua (e.g., from dust or charged particles). It will therefore be beneficial to first consider how polarization states are modelled before investigating the different physical processes responsible for polarized signals and the techniques used in subsequent analyses.

We consider the propagation of electromagnetic plane waves and define two waves propagating in the same direction $\mathbf{n}$ with

$$\mathbf{E}_1 = \mathbf{e}_1 E_1 e^{i(\mathbf{k}\cdot\mathbf{x}-\omega t)} \tag{1.1}$$

$$\mathbf{E}_2 = \mathbf{e}_2 E_2 e^{i(\mathbf{k}\cdot\mathbf{x}-\omega t)} \tag{1.2}$$

$$\mathbf{B}_j = \sqrt{\mu\epsilon}\,\mathbf{n}\times\mathbf{E}_j, \tag{1.3}$$

where $\mathbf{e}_1$, $\mathbf{e}_2$ and $\mathbf{n}$ are orthogonal unit basis vectors, $j = 1$ or 2, the constants E_1 and E_2 are complex, and $\mathbf{k} = k\mathbf{n}$. The superposition of these electromagnetic fields can be interpreted as a single wave characterized by a total electric field $\mathbf{E}(\mathbf{x}, t)$

$$\mathbf{E}(\mathbf{x}, t) = (\mathbf{e}_1 E_1 + \mathbf{e}_2 E_2)\, e^{i(\mathbf{k}\cdot\mathbf{x}-\omega t)}. \tag{1.4}$$

It is important to note that because E_1 and E_2 are complex quantities it is possible that phase differences will exist between the two components of the total electric field. In general, a phase difference will render the overall wave **elliptically polarized**. That is, the tip of the electric field vector is seen to be describing the figure of an ellipse over the interval of a period ($= 2\pi/\omega$). An important case is that of **linear polarization**, which happens when the two components share the same phase. It is then seen that the total electric field will be oriented at an angle

$$\theta = \arctan\left[\frac{\mathrm{Re}\,(E_2)}{\mathrm{Re}\,(E_1)}\right] \tag{1.5}$$

relative to the $\mathbf{e}_1$ unit basis vector ($\mathrm{Re}\,(\cdots)$ stands for the real part). On the other hand, we have **circular polarization** when E_1 and E_2 have the same amplitude, but are out-of-phase by $\pm\pi/2$. Equation (1.4) is then written as

$$\mathbf{E}\,(\mathbf{x},t) = E_1\,(\mathbf{e}_1 \pm i\mathbf{e}_2)\,e^{i(\mathbf{k}\cdot\mathbf{x}-\omega t)} \tag{1.6}$$

Taking the real part for both components, we find that the angle made by the electric field in relation to the $\mathbf{e}_1$-axis is a function of time with

$$\begin{aligned}\theta\,(t) &= \arctan\left[\frac{\mathrm{Re}\,(E_2)}{\mathrm{Re}\,(E_1)}\right] \\ &= \mp\arctan\left[\frac{\sin\,(\mathbf{k}\cdot\mathbf{x}-\omega t)}{\cos\,(\mathbf{k}\cdot\mathbf{x}-\omega t)}\right] \\ &= \mp\,(\mathbf{k}\cdot\mathbf{x}-\omega t)\,. \end{aligned} \tag{1.7}$$

At a given stationary point $\mathbf{x}$ in space, the electric field will sweep a circle at the angular frequency ω. If, for example, we set $\mathbf{e}_1 = \mathbf{e}_x$, $\mathbf{e}_2 = \mathbf{e}_y$, and $\mathbf{n} = \mathbf{e}_z$, then at a point z the electric field is rotating counter-clockwise in the xy-plane, as seen by an observer facing the incoming wave, and is said to be right circularly polarized for the "+" sign in equation (1.6)[1] ("−" in equation 1.7), and left circularly polarized for the "−" ("+" in equation 1.7).

Just as the unit vectors $(\mathbf{e}_1, \mathbf{e}_2, \mathbf{n})$ form a basis for a plane wave, an alternative basis can be built using the *circularly polarized basis vectors* $\mathbf{e}_\pm$ defined with

$$\mathbf{e}_\pm = \frac{1}{\sqrt{2}}\,(\mathbf{e}_1 \pm i\mathbf{e}_2)\,, \tag{1.8}$$

and the vector $\mathbf{n}$. That these three vectors form a complete basis can be verified with the following relations

$$\mathbf{e}^*_\pm \cdot \mathbf{e}_\mp = 0 \tag{1.9}$$

$$\mathbf{e}^*_\pm \cdot \mathbf{n} = 0 \tag{1.10}$$

$$\mathbf{e}^*_\pm \cdot \mathbf{e}_\pm = 1, \tag{1.11}$$

and any vector, such as the electric vector, can be written using this basis

$$\mathbf{E}\,(\mathbf{x},t) = (\mathbf{e}_+ E_+ + \mathbf{e}_- E_-)\,e^{i(\mathbf{k}\cdot\mathbf{x}-\omega t)} \tag{1.12}$$

with the complex amplitudes

$$E_+ = \frac{1}{\sqrt{2}}\,(E_1 - iE_2) \tag{1.13}$$

$$E_- = \frac{1}{\sqrt{2}}\,(E_1 + iE_2)\,. \tag{1.14}$$

[1] This definition is in accordance with the IAU convention.

The **Stokes parameters** are a set of four parameters that allow the characterization of the polarization state of a beam of radiation, which is, of course, nothing more than a superposition of plane waves (through the Fourier transform). The amplitude of the electric field along the different basis vectors (perpendicular to the direction of propagation) are given by $\mathbf{e}_1 \cdot \mathbf{E}$ and $\mathbf{e}_2 \cdot \mathbf{E}$ for linear polarizations along $\mathbf{e}_1$ and $\mathbf{e}_2$, and $\mathbf{e}_+^* \cdot \mathbf{E}$ and $\mathbf{e}_-^* \cdot \mathbf{E}$ for right ($\mathbf{e}_+$) and left ($\mathbf{e}_-$) circular polarizations, respectively. Please note the use of the complex conjugate, as is usually done for the scalar product between complex quantities. If we define these amplitudes, using equations (1.4) and (1.12), as

$$E_j = a_j e^{i\delta_j} \tag{1.15}$$
$$E_\pm = a_\pm e^{i\delta_\pm} \tag{1.16}$$

with $j = 1, 2$, then the Stokes parameters[2] are given by

$$\begin{aligned} I &= |\mathbf{e}_1 \cdot \mathbf{E}|^2 + |\mathbf{e}_2 \cdot \mathbf{E}|^2 \\ &= a_1^2 + a_2^2 && (1.17) \\ Q &= |\mathbf{e}_1 \cdot \mathbf{E}|^2 - |\mathbf{e}_2 \cdot \mathbf{E}|^2 \\ &= a_2^2 - a_1^2 && (1.18) \\ U &= 2\,\mathrm{Re}\left[(\mathbf{e}_1 \cdot \mathbf{E})^* (\mathbf{e}_2 \cdot \mathbf{E})\right] \\ &= 2\,a_1 a_2 \cos(\delta_2 - \delta_1) && (1.19) \\ V &= 2\,\mathrm{Im}\left[(\mathbf{e}_1 \cdot \mathbf{E})^* (\mathbf{e}_2 \cdot \mathbf{E})\right] \\ &= 2\,a_1 a_2 \sin(\delta_2 - \delta_1) && (1.20) \end{aligned}$$

when using the $(\mathbf{e}_1, \mathbf{e}_2)$ basis, and by

$$\begin{aligned} I &= \left|\mathbf{e}_+^* \cdot \mathbf{E}\right|^2 + \left|\mathbf{e}_-^* \cdot \mathbf{E}\right|^2 \\ &= a_+^2 + a_-^2 && (1.21) \\ Q &= 2\,\mathrm{Re}\left[\left(\mathbf{e}_+^* \cdot \mathbf{E}\right)^* \left(\mathbf{e}_-^* \cdot \mathbf{E}\right)\right] \\ &= 2\,a_+ a_- \cos(\delta_- - \delta_+) && (1.22) \\ U &= 2\,\mathrm{Im}\left[\left(\mathbf{e}_+^* \cdot \mathbf{E}\right)^* \left(\mathbf{e}_-^* \cdot \mathbf{E}\right)\right] \\ &= 2\,a_+ a_- \sin(\delta_- - \delta_+) && (1.23) \\ V &= \left|\mathbf{e}_+^* \cdot \mathbf{E}\right|^2 - \left|\mathbf{e}_-^* \cdot \mathbf{E}\right|^2 \\ &= a_+^2 - a_-^2 && (1.24) \end{aligned}$$

when using the $(\mathbf{e}_+, \mathbf{e}_-)$ basis. It is apparent from the second of equation (1.18) that Q is a measure of the amount linear polarization, and from equation (1.24) that V is

[2] It would be more precise to write $I \propto |\mathbf{e}_1 \cdot \mathbf{E}|^2 + |\mathbf{e}_2 \cdot \mathbf{E}|^2$, etc., since one is usually concerned with intensities or power, not (the square of) electric fields. However, these definitions will be adequate for the purpose of our discussion.

a measure of the amount of circular polarization. Both sets of equations make it clear that I is (proportional to) the total intensity of radiation, irrespective of the polarization basis. It can be shown that U is also a measure of linear polarization, but along axes oriented at 45 deg from $\mathbf{e}_1$ and $\mathbf{e}_2$ (see the exercise below).

It can also be readily verified that the intensity of radiation I is related to the other Stokes parameters by

$$I^2 = Q^2 + U^2 + V^2. \tag{1.25}$$

It is important to realize, however, that this last relation is only valid for purely deterministic and monochromatic signals. In general, radiation comes in the form of beams of finite duration (as opposed to a single plane wave) and are, therefore, not monochromatic, and can also only be partially polarized (either linearly, circularly, or both). Then, equation (1.25) must in general be replaced with

$$I^2 \leq Q^2 + U^2 + V^2. \tag{1.26}$$

Exercise 1.1. Define a new basis oriented at 45 deg from $\mathbf{e}_1$ and $\mathbf{e}_2$ with

$$\mathbf{e}_{/} = \frac{1}{\sqrt{2}}\left(\mathbf{e}_1 + \mathbf{e}_2\right) \tag{1.27}$$

$$\mathbf{e}_{\backslash} = \frac{1}{\sqrt{2}}\left(\mathbf{e}_1 - \mathbf{e}_2\right) \tag{1.28}$$

and show that

$$\mathbf{E}\left(\mathbf{x}, t\right) = \left(\mathbf{e}_{/} E_{/} + \mathbf{e}_{\backslash} E_{\backslash}\right) e^{i(\mathbf{k}\cdot\mathbf{x} - \omega t)} \tag{1.29}$$

with

$$E_{/} = \frac{1}{\sqrt{2}}\left(E_1 + E_2\right) \tag{1.30}$$

$$E_{\backslash} = \frac{1}{\sqrt{2}}\left(E_1 - E_2\right) \tag{1.31}$$

as well as

$$\begin{aligned} I &= \left|\mathbf{e}_{/}\cdot\mathbf{E}\right|^2 + \left|\mathbf{e}_{\backslash}\cdot\mathbf{E}\right|^2 \\ &= a_1^2 + a_2^2 \qquad (1.32) \\ Q &= 2\,\mathrm{Re}\left[\left(\mathbf{e}_{\backslash}\cdot\mathbf{E}\right)^*\left(\mathbf{e}_{/}\cdot\mathbf{E}\right)\right] \\ &= a_2^2 - a_1^2 \qquad (1.33) \\ U &= \left|\mathbf{e}_{/}\cdot\mathbf{E}\right|^2 - \left|\mathbf{e}_{\backslash}\cdot\mathbf{E}\right|^2 \\ &= 2\,a_1 a_2 \cos\left(\delta_2 - \delta_1\right) \qquad (1.34) \\ V &= 2\,\mathrm{Im}\left[\left(\mathbf{e}_{\backslash}\cdot\mathbf{E}\right)^*\left(\mathbf{e}_{/}\cdot\mathbf{E}\right)\right] \\ &= 2\,a_1 a_2 \sin\left(\delta_2 - \delta_1\right). \qquad (1.35) \end{aligned}$$

This result shows that the Stokes parameter U is indeed measure of linear polarization along axes oriented at 45 deg from $\mathbf{e}_1$ and $\mathbf{e}_2$.

Combining the results from the three different bases, it is perhaps helpful and more intuitive to express the Stokes parameters with

$$I = \left|\mathbf{e}_{1,+,/} \cdot \mathbf{E}\right|^2 + \left|\mathbf{e}_{2,-,\backslash} \cdot \mathbf{E}\right|^2 \tag{1.36}$$
$$Q = \left|\mathbf{e}_1 \cdot \mathbf{E}\right|^2 - \left|\mathbf{e}_2 \cdot \mathbf{E}\right|^2 \tag{1.37}$$
$$U = \left|\mathbf{e}_{/} \cdot \mathbf{E}\right|^2 - \left|\mathbf{e}_{\backslash} \cdot \mathbf{E}\right|^2 \tag{1.38}$$
$$V = \left|\mathbf{e}_{+}^* \cdot \mathbf{E}\right|^2 - \left|\mathbf{e}_{-}^* \cdot \mathbf{E}\right|^2, \tag{1.39}$$

where the nature of each quantity is clearly noticed.

In cases where there is no circular polarization (i.e. $V = 0$), which is sometimes a warranted assumption, we can express the polarized component of the electric field as

$$\mathbf{E}_p(\mathbf{x}, t) = E_p\left(\mathbf{e}_1 \cos\theta + \mathbf{e}_2 \sin\theta\right) e^{i(\mathbf{k}\cdot\mathbf{x} - \omega t)}, \tag{1.40}$$

which, using our definitions for the Stokes parameters (see equations 1.18-1.19), yields

$$Q = I_p \cos(2\theta) \tag{1.41}$$
$$U = I_p \sin(2\theta) \tag{1.42}$$

with the polarized intensity $I_p = E_p^2$. Note the dependency on 2θ (not θ).

Polarization measurements, especially linear polarization, are often presented using the **polarization fraction** (or **percentage**, or **level**) p and the **polarization angle** (let us again use θ but other definitions are often adopted; we will use Φ later on)

$$p = \frac{\sqrt{Q^2 + U^2}}{I} \tag{1.43}$$
$$\theta = \frac{1}{2} \arctan\left(\frac{U}{Q}\right). \tag{1.44}$$

The combination of these two parameters lend themselves well to the notion of a **polarization (pseudo-)vector**, where the length of the vector is set by p and its orientation (which is not a direction) by θ. One must, however, by careful with this analogy because these pseudo-vectors do not behave like normal vectors. For example,

- two polarization measurements yielding the same level p and orientations differing by $\pi/2$ do not add up to give a total vector of length $\sqrt{2}p$ and of intermediate orientation. Instead equations (1.41)-(1.42) make it clear the resulting polarization pseudo-vector will be of length $p = 0$ since $\cos(2\theta) + \cos(2\theta + \pi) = \sin(2\theta) + \sin(2\theta + \pi) = 0$. In other words, polarization pseudo-vectors exhibiting the same level p and orientated perpendicular to one another cancel out.

- Although p and θ lend themselves well for certain types of analysis, it is important to remember that Q and U are the fundamental quantities that should be manipulated for calculations performed at the fundamental level. For example, if two sets of polarization measurements made on the same source are to be combined to, say, improve the signal-to-noise ratio, then it is the Q and U parameters that must be averaged, not p and θ.
- Finally, the polarization angle is generally defined such $\theta = 0$ when pointing north on the sky and is increasing eastward ($0 \leq \theta \leq \pi$).

1.2 Polarization from spectral lines

$\Rightarrow$ *Individual spectral lines from atoms or molecules are intrinsically polarized, but...* $\Leftarrow$

Let us consider the case, for example, of a simple molecule (e.g., as carbon monoxide (CO)) with rotational states $|J, m\rangle$ defined by the quantum numbers J and m, with $-J \leq m \leq J$ in steps of 1. We will assume, for simplicity, that the molecule is in the electronic and vibrational ground states such that we are only dealing with pure rotational transitions. A transition $|J, m\rangle \rightarrow |J + \Delta J, m + \Delta m\rangle$ will be allowed for cases where $\Delta J = \pm 1$ and $\Delta m = 0, \pm 1$; an example is provided in Figure 1.1. The nature of the polarization state of a given spectral line depends on the value Δm, the change in the magnetic quantum number. More precisely, a so-called π-line will result when $\Delta m = 0$ and a σ-line whenever $\Delta m = \pm 1$ (i.e., there are two of them).

A group of atoms or molecules must somehow be aligned in order to exhibit detectable polarized emission (or absorption) from a given spectral line, i.e., their symmetry axis must have a preferential orientation in relation to some external agent. An ambient magnetic field pervading the region within which the atoms/molecules are located will serve such a purpose, as long as a few conditions are met:

- The atoms/molecules under question are endowed with a magnetic moment. Certainly, this will be the case for molecules to soon be discussed within the context of the Zeeman effect (e.g., HI, OH and CN) since, as we will see, the frequency splitting at the heart of this effect comes from a magnetic dipolar interaction. However, even other molecules weakly sensitive to the Zeeman effect (e.g., CO, CS, H_2O, ...) will also have a small magnetic moment due to the rotation of their nuclei (and their "slipping" from the electrons).
- If the magnetic moment μ and the ambient magnetic field strength B are such that $\mu B/\hbar > \nu_{\rm coll}, A_{ul}, B_{ul}I$, with $\nu_{\rm coll}$ the collisional rate and A_{ul} and $B_{ul}I$ the spontaneous and stimulated emission rates, then the molecules will be effectively aligned by the magnetic field. This condition usually easily met in a wide range of environments. For example, for molecules like CO we have $\mu/\hbar \sim 1$ mH/μG while at a density of, say, $n \sim 10^4$ cm^{-3} and a relative collision velocity of $\Delta v \sim 1$ km/sec $\nu_{\rm coll} \approx n\sigma\Delta v \approx 10^{-6}$ s^{-1} (i.e., $\sigma \sim 10^{-15}$ cm^2), as well $A_{ul} \sim 10^{-6}$ s^{-1} for CO ($J = 2 \rightarrow 1$). That is, even a weak magnetic field of $B \sim 10\,\mu$G will easily meet this condition.

When these conditions are met, the magnetic field orientation defines a natural axis for quantization. As depicted in Figure 1.1, it then follows that the π- and σ-lines spectral lines all have different polarization characteristics as well as radiation patterns in relation to the external magnetic field orientation. Namely,

- The π-line (when $\Delta m = 0$) only emits linearly polarized radiation aligned with the external magnetic field and a radiation pattern perpendicular to it. For example, an observer detecting emission from a π-line when the external magnetic field is confined to the plane of the sky would see the corresponding spectral line as being linearly polarized in the same direction as the field. On the other hand, the π-line would not be detected if the magnetic field was (anti-)parallel with the line of sight. At intermediate orientation for the magnetic field, the radiation from the π-line would be polarized along the orientation of the projected magnetic field on the plane of the sky.

- Radiation from the σ-lines (when $\Delta m = \pm 1$) is generally elliptically polarized, with their common linear polarization component perpendicular to that of the π-line (i.e., perpendicular to the orientation of the projected magnetic field on the plane of the sky). The two σ-lines have, however, opposite circular polarization states (i.e., right for $\Delta m = +1$ and left for $\Delta m = -1$ when the field is pointing at the observer, and vice-versa). The detected polarization for a given σ-line is purely linear when the magnetic field is confined to the plane of the sky and purely circular (anti-)parallel with the line of sight.

Given the differences in the polarization properties and radiation patterns, as well as their close relation to the orientation of the external magnetic field, one might expect that it would be easy to characterize the magnetic field through polarization measurements. As it turns out, this is far from being the case... One can identify a few obstacles:

- At thermodynamic equilibrium both σ-lines have the same intensity and their total intensity equals that of the π-line. If all these lines happen at the same (or are close in) frequency, then their polarization pseudo-vectors will cancel out because there would then be an equal intensity or radiation in perpendicular radiation states (see then end of Sec. 1.1). The lack of a polarization signal implies the impossibility of measuring the orientation of the projected magnetic field on the plane of the sky.

- Because the two σ-lines share the same radiation pattern and their circular polarization signals are opposite (i.e., orthogonal) no net polarization can be detected whenever these lines fall at the same (or are close in) frequency. Under these conditions we cannot expect to learn anything concerning the line of sight component of the magnetic field.

Since both of these issues appear to be linked to the fact that the π- and σ-lines *i)* fall close in frequency and *ii)* are related in their intensities and radiation patterns, maybe we can hope to make progress by identifying physical processes that mitigate these issues.

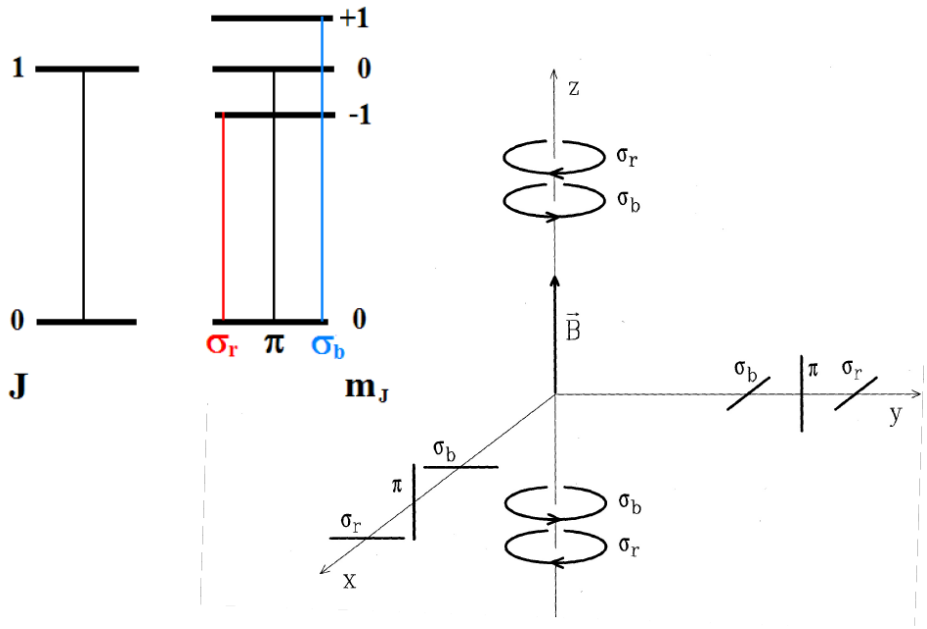

Figure 1.1: Energy levels for the $J = 0, 1$ rotational state of the, for example, CO molecule (left) and the possible transitions between the two sets of states (right). The presence of a magnetic field **B** will lift the degeneracies between the levels and provide a natural quantization axis. An ensemble of molecules will preferentially aligned themselves relative to orientation of the magnetic field, which is essential for the existence of a net polarization signal in the radiation emanating from the ensemble of molecules. Courtesy R. M. Crutcher.

1.2.1 The Zeeman effect

> In the absence of a magnetic field the period of all these oscillations is the same. But as soon as the electron is exposed to the effect of a magnetic field, its motion changes. - Pieter Zeeman

If we consider a classical electron of charge q and mass m_e exhibiting some orbital motion in an atom or a molecule, then we can calculate its magnetic moment μ by the product of the associated electric current and the area contained within the circuit traced by the charge. Assuming a circular orbit we have

$$\begin{aligned} \mu &= q\frac{\omega}{2\pi} \cdot \pi r^2 \\ &= \frac{q}{2m_e} m_e v r \\ &= \frac{q}{2m_e} L, \end{aligned} \tag{1.45}$$

where we used $v = \omega r$ for the orbital speed and L is the angular momentum (here, I follow the usual custom of denoting the electronic angular momentum by L instead of J, which is for the total angular momentum). We therefore see that the magnetic moment of the electron is proportional to its angular momentum. When the atom or molecule is subjected to an external magnetic (induction) field $\mathbf{B}$ the Hamiltonian of the system can be written

$$H = H_0 - \boldsymbol{\mu} \cdot \mathbf{B}, \tag{1.46}$$

where H_0 is the Hamiltonian of the free atom or molecule (i.e., when unperturbed by the external field) and we have generalized the field-matter interaction using the total (vectorial) magnetic moment $\boldsymbol{\mu}$, which potentially contains a contribution from all the components (i.e., particles) of the system.

If we now define the magnetic field as being oriented along the z-axis, i.e., $\mathbf{B} = B\mathbf{e}_z$, then for the simple case where only one electron contributes to the total magnetic moment

$$H = H_0 - \frac{\mu_\mathrm{B}}{\hbar} L_z B, \tag{1.47}$$

with the **Bohr magneton**

$$\mu_\mathrm{B} = \frac{q\hbar}{2m_\mathrm{e}}. \tag{1.48}$$

We now transition to the quantum world and write

$$\begin{aligned} \hat{H} &= \hat{H}_0 - \hat{\boldsymbol{\mu}} \cdot \mathbf{B} \\ &= \hat{H}_0 - \frac{\mu_\mathrm{B}}{\hbar} \hat{L}_z B, \end{aligned} \tag{1.49}$$

where we still treat the magnetic field as a classical entity (for that reason analyses such as this one are often called "semi-classical"). Assuming that $\hat{H}_0$ has the set $\{|\ell, m\rangle\}$ for its eigenvector with the eigenvalue, say, $E_{\ell,m}$, we find that the interaction with the magnetic field changes this energy by an amount

$$\Delta E_{\ell,m} = -\mu_\mathrm{B} m B. \tag{1.50}$$

We therefore find that the energy of the system is altered by a quantity that is proportional to the **magnetic quantum number** m and the external magnetic field. This is a very important example as it clearly shows that the $2\ell + 1$ times degeneracy of the $|\ell, m\rangle$ state is lifted by the presence of the magnetic field. For an atom or molecule, this implies that a spectral line associated with the **principal quantum number** ℓ should split into $2\ell + 1$ separate **fine structure** lines. This is the so-called **normal Zeeman effect**.[3]

[3] Although we have considered a "one-electron" atom (at least, as far as the external interaction is concerned), this formalism can be extended to any quantum mechanical system possessing a magnetic moment.

Although this effect is observed experimentally, it does not account for all possible results. For example, for systems where $\ell = 0$ (and therefore $m = 0$) it is found (e.g., for the hydrogen atom) that there can still exist a spectral splitting, contrary to what would be expected through equation (1.50). For this reason, this is called the **anomalous Zeeman effect**.

It was found that this effect could be explained if one postulates that the electron (and other particles) possesses an **intrinsic angular momentum** or **spin** $\hat{\mathbf{S}}$, to which an intrinsic magnetic moment is associated

$$\hat{\boldsymbol{\mu}}_{\rm s} \simeq 2\frac{\mu_{\rm B}}{\hbar}\hat{\mathbf{S}}, \tag{1.51}$$

where the proportionality factor of 2 for the electron is precise to about 10^{-3}. Comparison with equations (1.45) and (1.48) reveals that the electron spin has a **gyromagnetic ratio** $\gamma \simeq 2\mu_{\rm B}/\hbar$ (and generally defined through $\hat{\boldsymbol{\mu}}_{\rm s} \equiv \gamma\hat{\mathbf{S}}$, or $\hat{\boldsymbol{\mu}} \equiv \gamma\hat{\mathbf{L}}$ in equation (1.45)) that is approximately twice that of its orbital angular momentum.

We therefore find that the Zeeman effect potentially solves one of the issues previously identified since it will ensure, in principle, that the π- and σ-lines do not fall at the same frequency. This will be true, at least, for atoms and molecules that are strongly sensitive to the Zeeman effect. We should therefore be looking for candidates that are *i)* abundant enough in the ISM and *ii)* have an odd number of electrons, thus ensuring the existence of a corresponding spin and a strong magnetic moment through equation (1.51) (a non-zero nuclear spin would unlikely be sufficient since the Bohr magneton is replaced by the nuclear magneton in that equation). For this reason, the main spectral lines used to probe the Zeeman effect in the ISM are atomic hydrogen (HI), hydroxyl (OH) and cyanid (CN), which all have $S = 1/2$.

Before we look more closely at some candidate spectral lines, let us look at what can be expected as far as solving our frequency degeneracy problem. The Zeeman sensitivity associated with these spectral transitions is on the order of 1 Hz/μG. Looking on the high-side of magnetic field strengths we can expect $B \sim 1$ mG in the denser parts of giant molecular clouds. That is, the **Zeeman splitting** between the π- and σ-lines will be $\Delta\nu_z \sim 1$ kHz. On the other hand, line of sight velocities measured for these spectral lines can often reach as high as tens of km/s. Using the Doppler shift formula we find that

$$\Delta\nu \approx 3.3\left(\frac{\nu_0}{1\ {\rm GHz}}\right)\left(\frac{\Delta v}{1\ {\rm km\ s^{-1}}}\right)\ {\rm kHz}, \tag{1.52}$$

where ν_0 and Δv are the frequency of the spectral transition and its line width, respectively.

We can therefore already see that, although π- and σ-lines will not fall on the same frequency for a given line of sight velocity, there will be significant spectral overlap between them. This effect, which gets worse with increasing frequency, will strongly limit the applicability of the Zeeman effect for measuring the magnetic field strength. For example, while the Doppler broadening would be on the order ~ 5 kHz with $\Delta v = 1$ km/s for the commonly used OH lines at 18 cm, it would become ~ 376 kHz for the CN

($N = 1 \rightarrow 0$) transition at 113 GHz. It should be apparent that we should not expect to often see a clear Zeeman splitting between the π- and σ-lines but rather a **Zeeman broadening** in most cases.

What are further consequences of this overlap? As we have seen in Sec. 1.1 the Stokes Q, U and V can be defined as subtractions of signals exhibiting two orthogonal polarization states: linear polarizations along $\mathbf{e}_1$ and $\mathbf{e}_2$ for Q (see equation 1.18) and along axes oriented at 45 deg from $\mathbf{e}_1$ and $\mathbf{e}_2$ for U (see equation 1.34); and circular polarizations along $\mathbf{e}_+$ and $\mathbf{e}_-$ for V (see equation 1.24). Whenever $\Delta\nu_z \ll \Delta\nu$ Taylor expansions can be used to transform these differences to

$$Q \simeq -\frac{1}{4}\frac{d^2I}{d\nu^2}\left(\cos\theta - \sin\theta\right)\left(\Delta\nu_z \sin\iota\right)^2 \tag{1.53}$$

$$U \simeq -\frac{1}{4}\frac{d^2I}{d\nu^2}\left(\sqrt{2}\sin\theta\right)\left(\Delta\nu_z \sin\iota\right)^2 \tag{1.54}$$

$$V \simeq \frac{dI}{d\nu}\Delta\nu_z \cos\iota, \tag{1.55}$$

with θ, as before, the polarization angle on the plane of the sky (relative to $\mathbf{e}_1$) and ι the inclination angle of the magnetic field relative to the line of sight (Crutcher et al. 1993, ApJ, 407, 175). It follows that

- The Stokes Q and U signals are proportional to the square of the plane-of-the-sky component of the magnetic field. However, because of their dependency on the second frequency derivative of the total intensity I they will be extremely weak and generally impossible to measure.
- The Stokes V spectrum is proportional to the first frequency derivative of the total intensity I as well as the line-of-sight component of the magnetic field, and can therefore yield its strength.

Despite these significant limitations, the Zeeman effect is still to this day the only means we have for *directly* measuring the strength of the magnetic field, i.e., its line of sight component. It therefore remains a powerful tool for studying magnetic fields in the ISM.

1.2.1.1 Zeeman measurements with HI, OH and CN

The transitions at 21-cm (1.42 GHz) for HI ($F = 1 \rightarrow 0$); 1.6-1.7 GHz (18-cm), 6 GHz, ..., for OH $\left({}^2\Pi_{3/2}, J = 3/2, 5/2, ...\right)$; and at 113 GHz for CN ($N = 1 \rightarrow 0$) have been the main tools for studying the Zeeman effect in the ISM. Each of the atom/molecules have an unpaired electron, which renders their transitions sensitive to the Zeeman effect. Figure 1.2 shows the energy level diagram for the HI 21-cm line in the presence of an external magnetic field responsible for the Zeeman splitting of the $F = 1$ sub-levels. Also shown are the three possible transitions $F = 1 \rightarrow 0$, which are magnetic dipolar in nature.

The 21-cm line is usually very broad in velocity with complicated line shapes. The Zeeman effect and, accordingly, measurements of the line-of-sight component of the magnetic

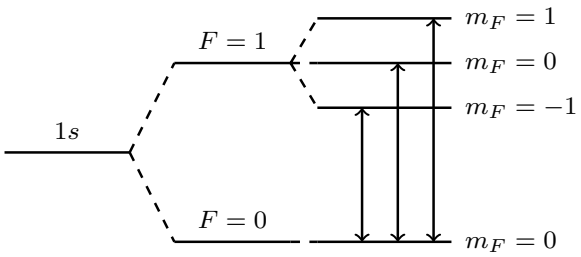

Figure 1.2: Energy level diagram for the HI 21-cm line in the presence of an external magnetic field responsible for the Zeeman splitting of the $F = 1$ sub-levels. From Rajabi & Houde 2016, ApJ, 826, 216.

field ($B_{\rm los}$) can thus be difficult to obtain. Example of successful detections (in absorption) toward the M17 HII region/M17 SW interface are shown in Figure 1.3. As can be seen, only a small portion of the spectra exhibited a Stokes V signal consistent with the Zeeman effect; yielding magnetic field strengths ranging from $\sim 100 - 500$ μG directed at the observer. The magnetic field strength are obtained by scaling the frequency derivative of the Stokes I signal (top panels) to the Stokes V spectrum (bottom panels) using the known sensitivity factor Z for the 21-cm spectral line. The scaling factor yields $\Delta\nu_z = ZB_{\rm los}$, from equation (1.55).

Figure 1.4 shows an energy diagram for OH in the vibronic (i.e., vibrational and electronic) ground state but without Zeeman splitting; some of the main (rotational) transitions are also indicated. Despite being a linear molecule OH is fairly complex spectroscopically due to the non-zero values for the electronic orbital angular momentum and spin, as well as the Λ-doubling (resulting in the '+' and '−' levels) and the hyperfine interaction (leading to the final F levels).

An example of a successful detection of the Zeeman effect in the OH 1667 GHz line (see Fig. 1.4) still in absorption in M17 is shown in Figure 1.5. Despite the noisy appearance of the Stokes V spectrum (bottom panel), this would be considered a strong detection yielding a 3σ measurement of $B_{\rm los} = 150 \pm 50$ μG; in the world of Zeeman observations a 2σ level is often considered a detection.

The CN molecule is rather simple linear molecule with a corresponding energy ladder complicated by the fact that the presence of the nuclear spin adds an hyperfine structure that is responsible for the existence of a large number of lines even for the fundamental transition $N = 1 \rightarrow 0$ at 113 GHz. The hyperfine components (a total of 9 for this transition, 7 of which are strong) have differing sensitivities to the Zeeman effect and can be stacked together to improve sensitivity and reduced instrumental effects that complicated these measurements (beam squint, etc.; see Crutcher et al. 1996, ApJ, 456, 217). An example of a successful Zeeman detection in this transition is shown in Figure 1.6 for the W3(OH) molecular cloud complex. The estimated magnetic field strength $B_{\rm los} = 1.10 \pm 0.33$ mG was approximately 1/5 of instrumental contribution!

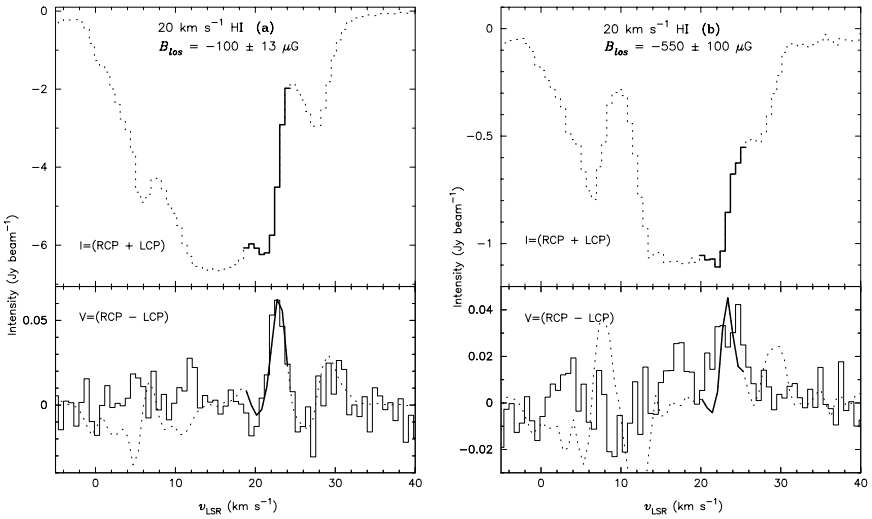

Figure 1.3: Measurements of the line-of-sight component of the magnetic field strength through circular polarization observations of the HI 21-cm line toward the M17 HII region/M17 SW interface. Stokes I and V spectra are shown in the top and bottom panels, respectively. In both cases, the best fit of the frequency derivative of the Stokes I signal to the Stokes V spectrum is shown with the solid curve and yields the corresponding value for $B_{\rm los}$. From Brogan et al. 2001, 560, 821.

Only the availability of the 7 strong hyperfine components could render a correction for the unwanted instrumental polarization possible (Falgarone et al. 2008, A&A, 487, 247).

The Zeeman detections presented here give us a good sense of the difficulties in realizing such measurements and, accordingly, the rate of new Zeeman detections has somewhat stagnated in recent years. However, the significant number of detections acquired through the years, combined with the unique information Zeeman measurements provide for magnetic field strengths, have yielded important results. For example, the aggregate of HI, OH and CN Zeeman measurements in diffuse and molecular clouds presented in Figure 1.7 have allowed us to effectively probe the sub/super-criticality of molecular clouds.

Finally, there are cases where Zeeman results are facilitated. This is sometimes true for some OH transitions when they are detected in the maser action regime. Masers often exhibit much narrower lines and are detected in regions of higher density harbouring stronger magnetic fields. A salient and unique example of this is shown in Figure 1.8 where the OH $\left({}^2\Pi_{3/2}, J = 7/2, F = 4^+ \rightarrow 4^-\right)$ line at 13.44 GHz was detected, also in W3(OH). In this case, the three observed maser lines are very narrow ($\Delta v \approx 0.3\,\mathrm{km\,s^{-1}}$ or $\approx$ 13 kHz) while the strong magnetic field ($B \simeq 7.6 - 10.6$ mG) brought about a clear Zeeman splitting $\Delta\nu_z \simeq 6 - 8.4$ kHz. In this unique instance for a molecular cloud, there is no need to compute a Stokes V spectrum from the two circular polarization

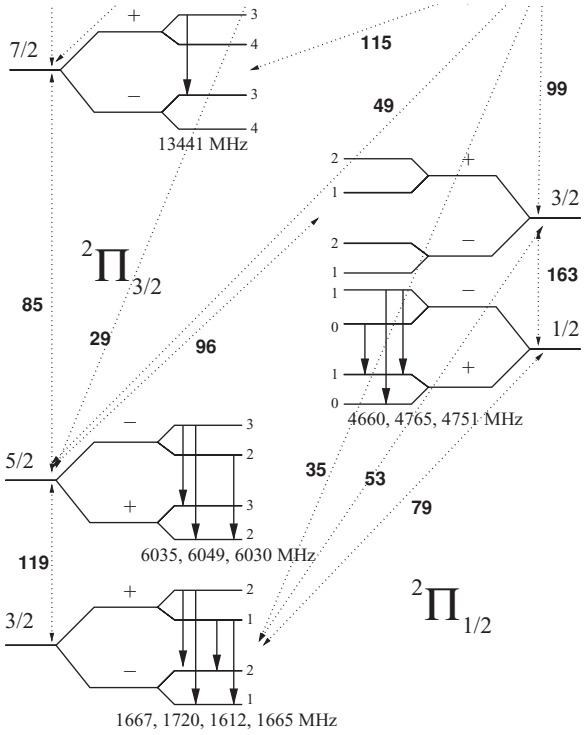

Figure 1.4: Energy levels up to $J = J' + N = 7/2$ in the vibronic ground state of OH. The levels are split into two ladders by spin–orbit coupling, with the left-hand ladder being $^2\Pi_{3/2}$ (i.e., $L = 1$, $S = 1/2$ and $J' = L+S = 3/2$), and the right-hand $^2\Pi_{1/2}$ (i.e., $J' = 1/2$). The rotational spacing is not to scale. These rotational levels are split by Λ-doubling into the '+' and '−' levels, while the hyperfine interaction ($I = 1/2$) is responsible for the further splitting of each lambda level into the final states denoted by $F = J + I$. These splittings are not drawn to scale and Zeeman splitting is not shown. From Gray 2012, Maser Sources in Astrophysics (New York: Cambridge Univ. Press).

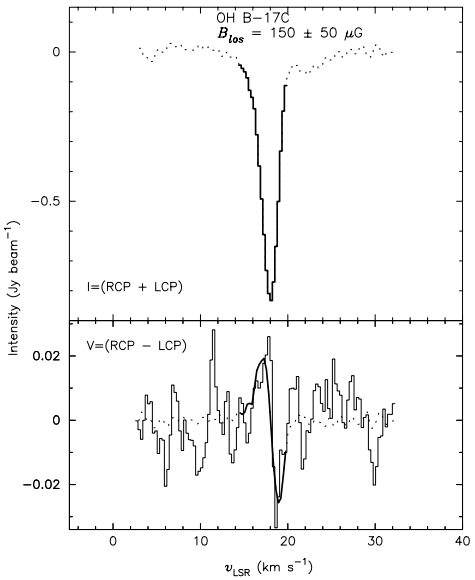

Figure 1.5: Same as Figure 1.3 but for the OH 1667 GHz line (see Fig. 1.4), still in absorption in M17. From Brogan et al. 2001, 560, 821.

measurements since the separation between them directly yields the *total* magnetic field strength (i.e., not $B_{\rm los}$) quoted above.

Why are these measurements atypical to what is usually seen in molecular clouds? The authors (Güsten, Fiebig and Uchida 1994, A&A, 26, L51) state that these observations suggest "*... a bow-shock model in which the magnetic field is compressed in the cooled post-shock layer preceding the compact HII region.*"

1.2.2 The Goldreich-Kylafis effect

We just saw that the Zeeman effect will cause large enough frequency shifts between the π- and σ-lines for some atomic or molecular transitions. But for the majority of molecules detected in the ISM this will not happen as their transitions are not Zeeman sensitive. In such cases, the widths of the spectral lines are much larger than the Zeeman broadening. For example, the Zeeman sensitivity of the CO ($J = 2 \rightarrow 1$) line is on the order of 1 mH/μG, i.e., a thousand times less than that for CN transitions. It follows that for all practical purposes we can consider the π- and σ-lines to fall at the same frequency, and we should not expect to be able to measure magnetic field strengths using the Zeeman effect with such spectral lines. This does not mean, however, that no manifestation of the effect the magnetic field has on a molecule can be detected under some circumstances.

For example, in the ISM under isotropic situations (and thermodynamic equilibrium) the magnetic sub-levels corresponding to different values for the quantum number m will have the same population and, as we already stated in Sec. 1.2, the superposition of the

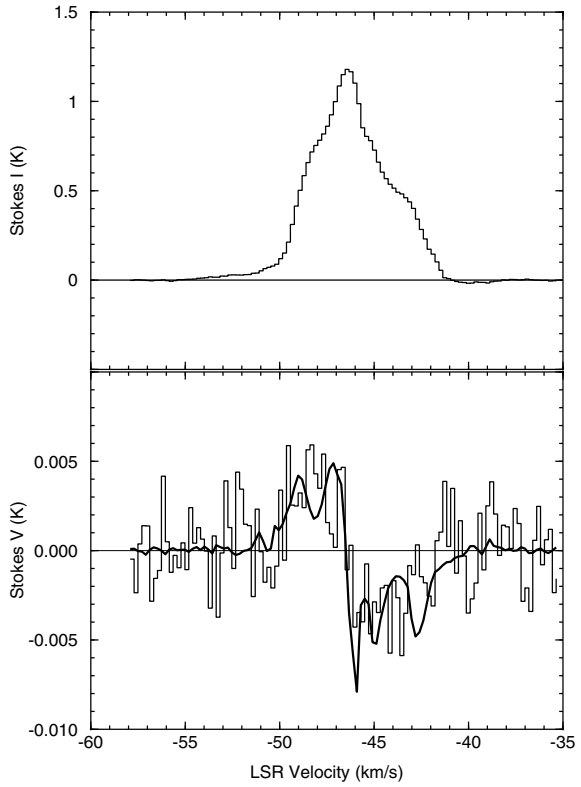

Figure 1.6: Zeeman detection in CN ($N = 1 \rightarrow 0$) at 113 GHz obtained for the W3(OH) molecular cloud complex. The estimated magnetic field strength $B_{\rm los} = 1.10 \pm 0.33$ mG was approximately $1/5$ of instrumental contribution. From Falgarone et al. 2008, A&A, 487, 247.

π- and σ-lines will result in net zero linear and circular polarization levels. However, if there is some anisotropy is present in the region harbouring the molecules, then the sub-level populations will come out of equilibrium and the corresponding change in intensity of the π-line relative to the σ-lines will result in a net, non-zero, linear polarization level.

How could this happen? Let us take a simple and concrete example and assume that the optical depth is not isotropic as seen by a population of molecules in a given region in the ISM. For example, let us assume that it is higher in directions collinear with the ambient magnetic field vector. A few consequences would result for this situation:

- Because the π-line radiates preferentially in directions perpendicular to the magnetic field, it will be more like to have σ-photons emitted by the molecules being absorbed on their path than π-photons, since these can also be emitted in directions collinear with the magnetic field.

- The sub-levels associated with changes $\Delta m = \pm 1$ will therefore become more pop-

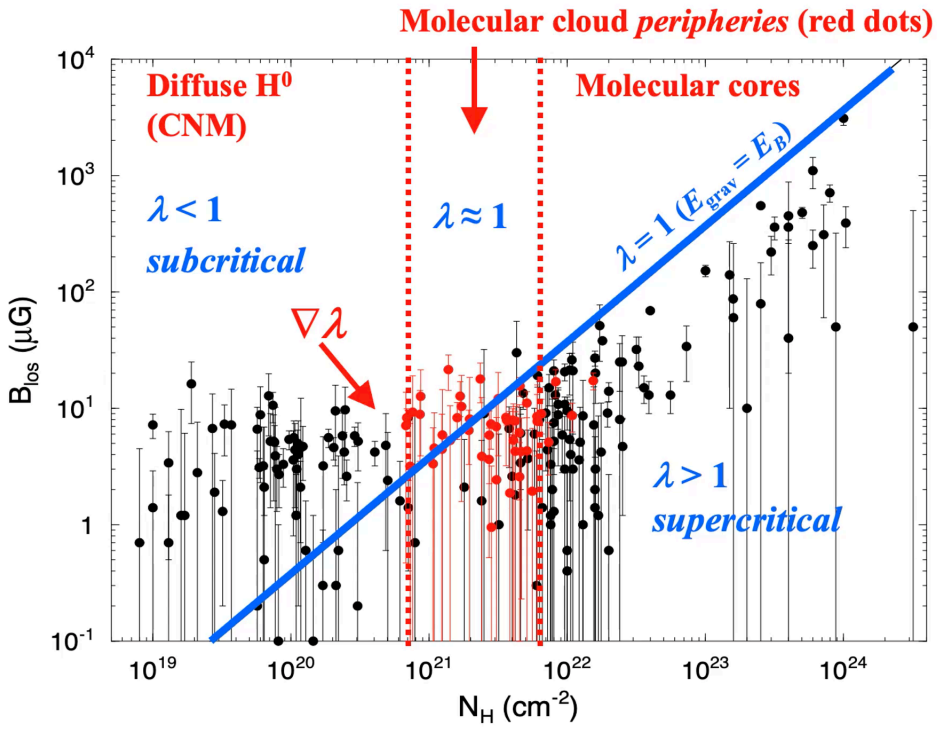

Figure 1.7: All HI, OH and CN Zeeman measurements obtained in diffuse and molecular clouds; magnetic field strength vs. column density. The blue line indicates the critical threshold for gravitational collapse ($\lambda = 1$) happens at a column density $N_{\rm H} \approx 10^{22}$ cm^{-2} (or a volume density $n_{\rm H} \approx 300$ cm^{-3}. Magnetic fields are strong enough to support clouds against gravity when $\lambda < 1$ (and vice-versa). Courtesy T. Troland, adapted from Crutcher et al. 2010, ApJ, 725, 466.

ulated than those responsible for $\Delta m = 0$.

- The radiation detected in directions perpendicular to the magnetic field will then tend to be dominated by the σ-lines, resulting in a net linear polarization orientation perpendicular to the magnetic field (on the plane of the sky).
- Evidently, the π-line would dominate in a situation where the optical depth is lower in directions collinear with the ambient magnetic field.
- The orientation of the projection of the magnetic field on the plane of the sky can be inferred by that of linear polarization pseudo-vector. There is, however, an inherent 90 deg ambiguity in the corresponding measurement.
- This effect reveals nothing concerning the strength of the magnetic field, at least not directly.

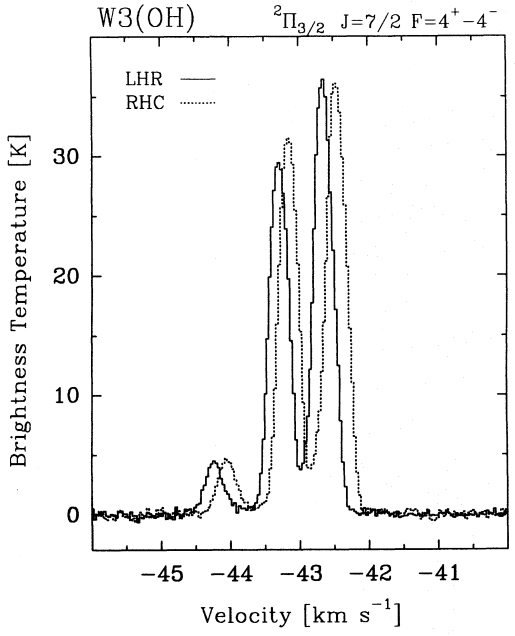

Figure 1.8: Detection of the Zeeman effect in OH $\left(^2\Pi_{3/2}, J = 7/2, F = 4^+ \rightarrow 4^-\right)$ lines in the W3(OH) molecular cloud complex. The combination of narrow spectral lines ($\Delta v \approx 0.3\,\mathrm{km\,s^{-1}}$ or ≈ 13 kHz) and strong *total* magnetic fields ($B \simeq 7.6 - 10.6$ mG) resulted in a clear Zeeman splitting $\Delta\nu_z \simeq 6 - 8.4$ kHz. From Güsten, Fiebig and Uchida 1994, A&A, 26, L51.

- No net circular polarization could ever be detected in any direction since it is not possible to differentiate between the σ-lines in this manner. This is because both lines have the same radiation pattern and happen at the same frequency.

In this example, the increased optical depth could be the result of a smaller velocity gradient in the chosen direction. However, any kind of anisotropy is likely to lead to the same effect. For example, an anisotropic external radiation field would also do the trick. This is the co-called *Goldreich-Kylafis effect* (Goldreich & Kylafis 1981, ApJ, 243, L75).

The polarization levels expected with Goldreich-Kylafis effect are fairly low, i.e, on the order of a few percent or less. Although it took 16 years before detecting linear polarization in rotational lines of molecules like CS and HCN consistent with the Goldreich-Kylafis effect (Glenn et al. 1997, ApJ, 487, L89; and soon after for CO), this is now routinely achieved with modern facilities and instruments. An example of a spectrum is shown in Figure 1.9 for the detection of linear polarization consistent with the Goldreich-Kylafis effect for the CO ($J = 2 \rightarrow 1$) spectral line at 230 GHz in Orion KL. Finally, a recent linear polarization map of NGC 6334 I(N) in CS ($J = 5 \rightarrow 4$) at 244.5 GHz (red vectors) obtained with ALMA is presented in Figure 1.10. Polarization from dust continuum at 1.3 mm (blue vectors) is also shown and will be discussed in Sec. 1.3, while

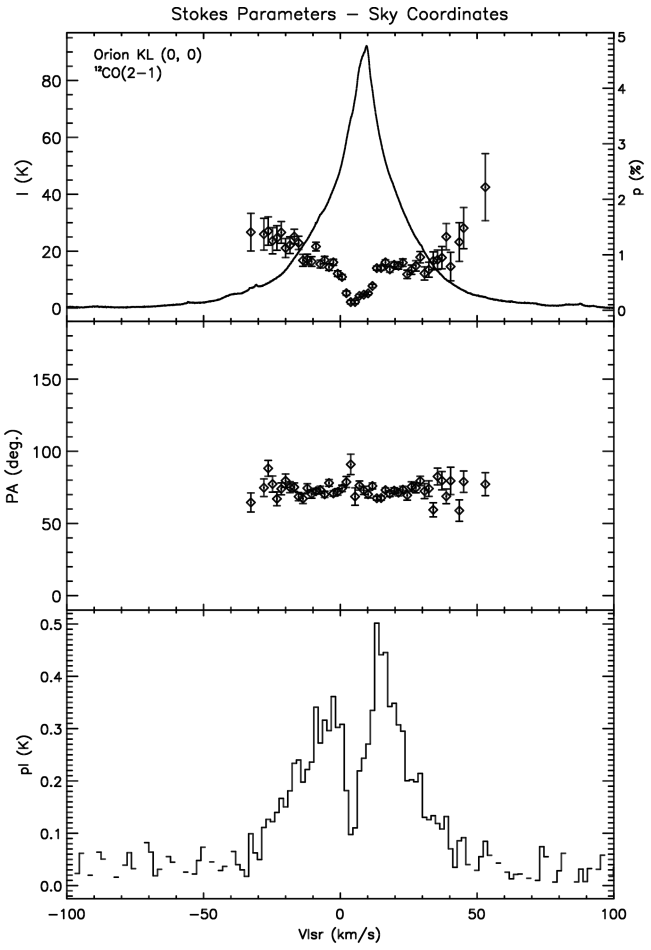

Figure 1.9: Measurement of linear polarization of the CO ($J = 2 \rightarrow 1$) spectral line at 230 GHz in Orion KL, consistent with the Goldreich-Kylafis effect. The top panel shows the Stokes I spectrum and polarization levels p (using the vertical axis on the right), the polarization angle in the middle panel and the polarized flux pI in the bottom. From Houde et al. 2013, ApJ, 764, 24.

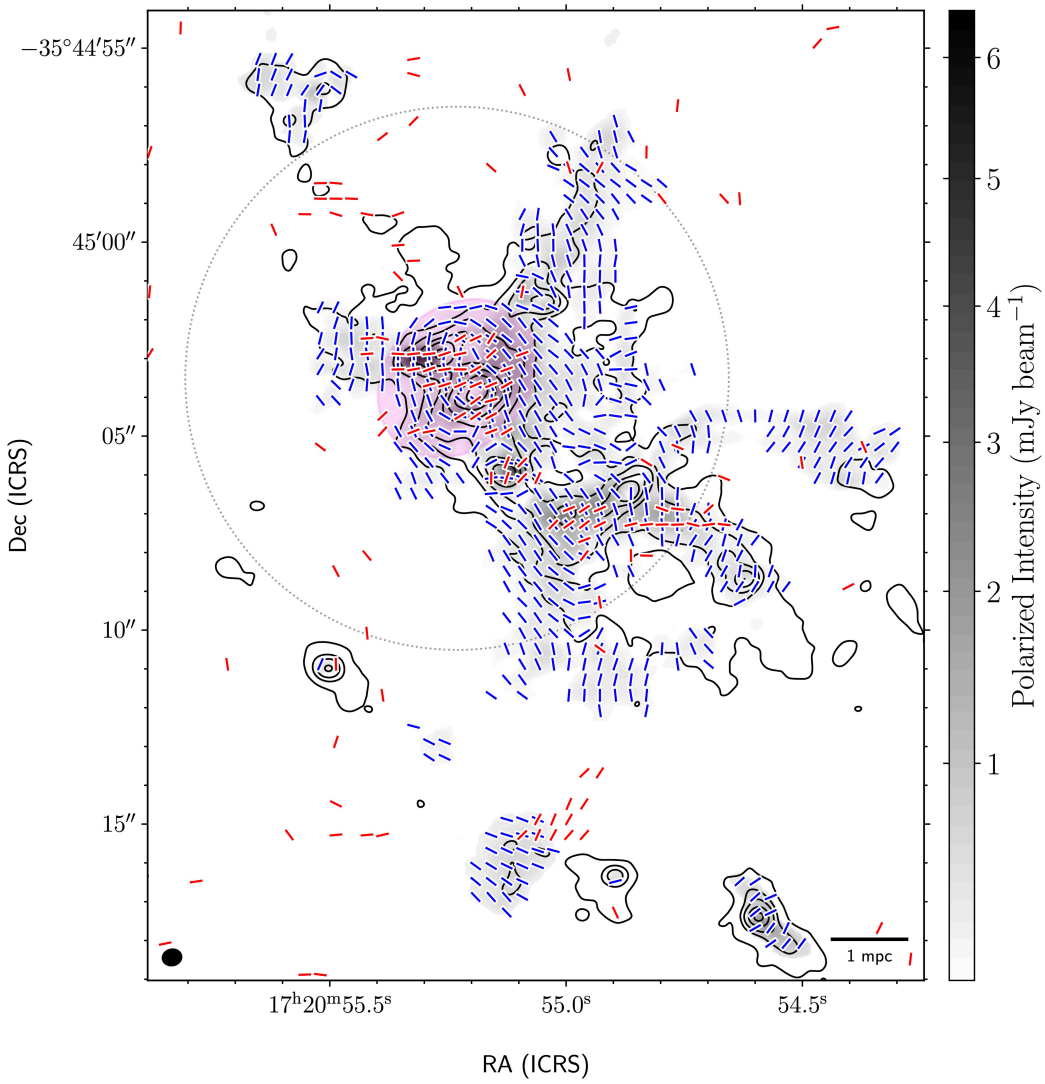

Figure 1.10: A linear polarization map of NGC 6334 I(N) in CS ($J = 5 \rightarrow 4$) at 244.5 GHz in red and in dust continuum at 1.3 mm in blue obtained with ALMA. Dust polarization, which reveals the magnetic field orientation on the plane of the sky, will be discussed in Sec. 1.3. From Cortés et al. 2021, ApJ, 923, 204.

we will discuss how information about magnetic fields and turbulence can be obtained from such maps in Sec. 1.5.1.

1.3 Polarization from dust

Dust grains in the ISM interact with radiation through scattering and absorption, and emit radiation at longer wavelengths. It has been known since the work of Hiltner more than 70 years ago that light from background stars is linearly polarized due to selective absorption by foreground dust. Likewise, subsequent work at far-infrared and mm/submm wavelengths has shown that radiation emanating from dust populations is also linearly polarized, albeit generally at 90 deg relative to that from background stars at shorter wavelengths.

Just as was the case for molecules discussed earlier, a population of grains can only radiate globally with a net level of polarization if its constituents are somehow aligned with some external agent. Here again, the external magnetic field will fulfill this role. The leading theory for grain alignment is the so-called Radiative Alignment Torque (RAT) theory (Lazarian & Hoang 2007, MNRAS, 378, 910), and its main ingredients can be listed as follows:

- Within the framework of RAT irregularities in the shapes of dust grains lead to a finite helicity which will serve to spin them up when irradiated by an external radiation field (we saw from equations 1.6 and 1.8 that an electric field can be expressed with two orthogonal circularly polarized states, which will scatter differently off the grains because of their helicity).

- Once a grain is spinning it will tend do so by minimizing its total energy while conserving its angular momentum, resulting in a rotation about its symmetry axis (i.e., the "short" axis, which has the maximum moment of inertia). This is the so-called internal alignment process, which is rendered possible through the Barnett effect where quantum mechanical unpaired spins (we are dealing with paramagnetic grains) flip to make up for the change in rotational angular momentum in the alignment process.

- Since the flipping of spins also brings about a net magnetization (there are initially as many pointing up than down), the grain will interact with the external magnetic field, resulting in its symmetry axis precessing about it.

- As different parts of the grain's surface are illuminated by the external radiation field the imparted radiative torques will tend to align its symmetry axis with the external magnetic field.

This brief description of grain alignment through RAT is admittedly oversimplified. A more careful treatment would, however, corroborate the conclusions that:

- In general, linear polarization from dust grain traces the orientation of the projection of the magnetic field on the plane of the sky.

- At short wavelengths (e.g., in the optical) where polarization is due to differential absorption, the linear polarization is aligned with the magnetic field.
- At longer wavelengths (e.g., at FIR and mm/summ wavelengths) where the radiation emanates from the grains, the linear polarization vectors are oriented at 90 deg relative to that of the magnetic field.
- The polarization level p is independent of the magnetic field strength (similar to the Goldreich-Kylafis effect but unlike the Zeeman effect) and varies proportionally to $\sin^2 \iota$.

Exercise 1.2. A toy model for the dependency of p on the inclination angle. A highly prolate dust grain is spinning at high rotational frequency ω while emitting in its own reference frame an electric field

$$\mathbf{E} = \left(\frac{E_0}{\sqrt{2}} + E_\parallel\right)\mathbf{e}_\parallel + \left(\frac{E_0}{\sqrt{2}} + E_\perp\right)\mathbf{e}_{\perp 1} + \left(\frac{E_0}{\sqrt{2}} + E_\perp\right)\mathbf{e}_{\perp 2}, \tag{1.56}$$

where $\mathbf{e}_\parallel$ is a unit vector aligned with the long axis of the grain, while $\mathbf{e}_{\perp 1}$ and $\mathbf{e}_{\perp 2}$ are each aligned with one of the two short axes and E_0 is the random unpolarized component of the field ($E_0 \gg E_\parallel, E_\perp$). Express the electric field in the reference frame of an observer whose line of sight is at an inclination angle ι relative to the symmetry axis of the grain and show that the polarization fraction can be written as

$$\begin{aligned} p(\iota) &= \frac{\left(I_\parallel - I_\perp\right)\sin^2\iota}{2I_0 + \left(I_\parallel + 3I_\perp\right) + \left(I_\parallel - I_\perp\right)\cos^2\iota} \\ &\simeq \frac{1}{2}\left(\frac{I_\parallel - I_\perp}{I_0}\right)\sin^2\iota, \end{aligned} \tag{1.57}$$

where $I_0 \propto \left\langle E_0^2 \right\rangle$, etc., with $\langle \cdots \rangle$ denoting an average. For this, you will also have to assume that E_0 is uncorrelated with $E_\parallel$ and $E_\perp$ (i.e., $\left\langle E_0 E_\parallel \right\rangle = \langle E_0 E_\perp \rangle = 0$), and that electric fields along different axes are also uncorrelated (i.e., $\left\langle E_\parallel E_\perp \right\rangle = \langle E_{\perp 1} E_{\perp 2} \rangle = 0$, etc.).

1.3.1 Dust polarization due to differential absorption (short wavelengths)

As stated earlier, light from background stars, assumed initially unpolarized, can become partially linearly polarized as it propagates through the ISM on its way to our telescopes. The process is illustrated in Figure 1.11. Because the component of the background starlight polarized along the long axis of the dust grains is preferentially absorbed the scattered electric field is polarized parallel to orientation of the plane of the sky component of the magnetic field responsible for the alignment of the grains.

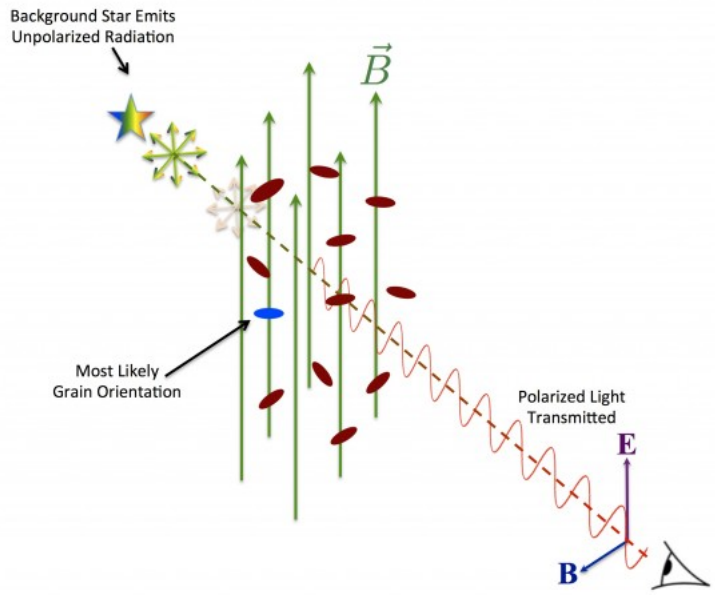

Figure 1.11: Cartoon showing the polarization of light from a background star as it propagates through the dense ISM. The radiation is initially unpolarized but becomes partially linearly polarized through differential absorption. The polarized electric field is aligned with plane of the sky component of the magnetic field.

Evidently there must be enough dust along the line of sight for the radiation to become polarized but not too much that the starlight is completely absorbed. Figure 1.12 shows images of the Bok globule (B68) at different wavelengths from blue to near-infrared bands. Background stars are more or less attenuated depending on the amount of dust along a line of sight and the wavelength of observation.

This technique of observations has a long been used to map the magnetic field over a vast range of scales. An example is shown in Figure 1.13, where linear polarization measurements reveal that the large scale magnetic field traces the Galactic plane at low latitude.

1.3.2 Dust polarization in emission (longer wavelengths)

Dust grains are heated up by the radiation they absorb at shorter wavelengths and release some of that energy by radiating at longer wavelengths (far-infrared and mm/submm). Because they emit more efficiently photons that are polarized along their long axis, the resulting electric field will be partially polarized in that orientation. The polarized signal is therefore aligned perpendicularly relative to the plane of the sky component of the magnetic field. This is illustrated in Figure 1.14. For this reason astronomers readily rotate polarization vectors by 90 deg to infer the orientation of the magnetic

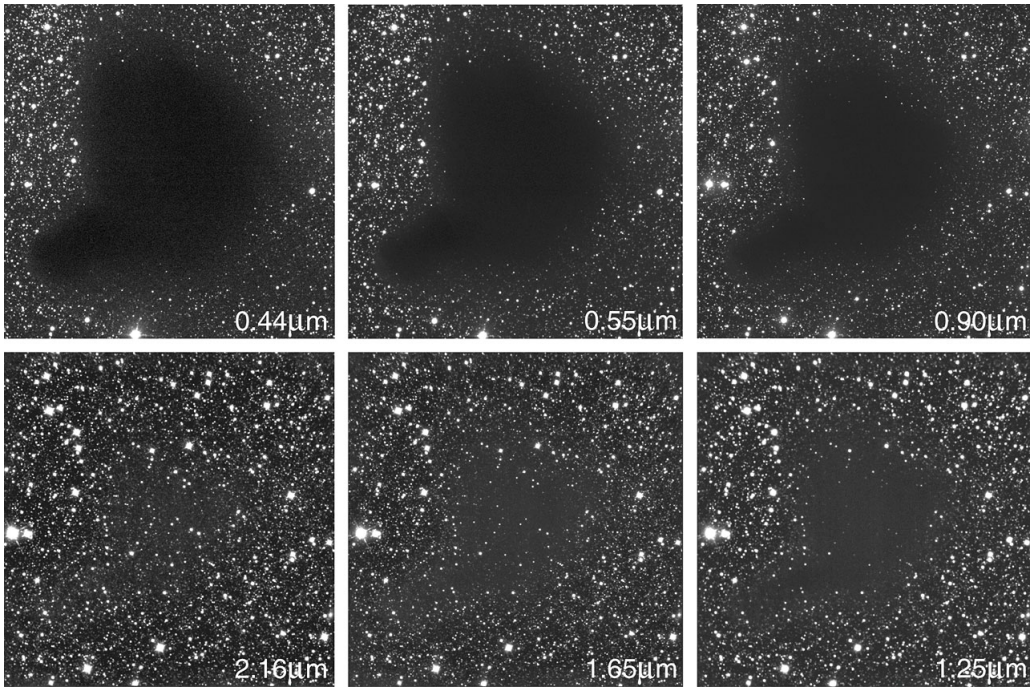

Figure 1.12: Images of the Bok globule (B68) at different wavelengths from the blue to the near-infrared. Background stars are more or less attenuated depending on the amount of dust along a line of sight and the wavelength of observation. Courtesy ESO.

field. Although this is usually warranted, one should always be careful...

We have shown earlier in Figure 1.10 an ALMA map of NGC 6334 I(N) combining dust polarimetry at 1.3 mm, therefore in emission (with the polarization vectors already rotated to show the magnetic field orientation), with CS ($J = 5 \rightarrow 4$) polarization at 244.5 GHz. Accounting for 90 deg ambiguity of the Goldreich-Kylafis effect, we can see that the two methods generally agree quite well. The agreement is also usually excellent between dust polarization measurements at short (differential absorption) and longer (emission) wavelengths. An example is given in Figure 1.15, where a polarimetry map of Serpens South from SOFIA/HAWC+ at 214 μm (emission; blue vectors) and with SIRPOL in the near-infrared (H band) (differential absorption; grey vectors) is presented, with both data sets showing the orientation of the magnetic field on the plane of the sky. We can further attest from this map that not only are the two types of measurements in good agreement but they are also nicely complementary. Polarization from dust emission traces the inner part of source while the differential absorption data maps the magnetic field on the large scale.

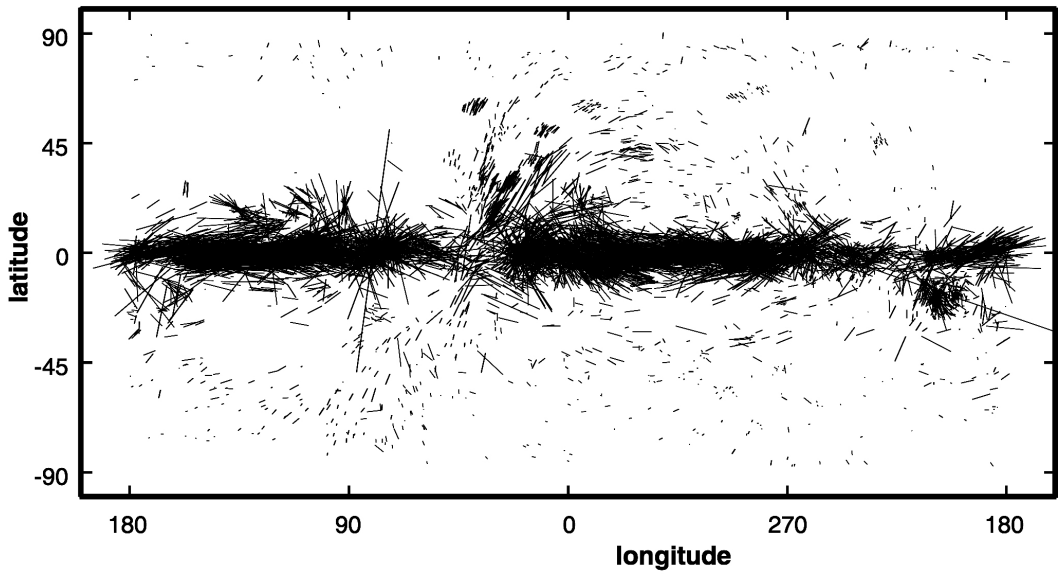

Figure 1.13: Starlight polarization measurements over the sky. At low latitudes the inferred orientation of the magnetic field follows the Galactic plane. Courtesy T. J. Jones.

1.4 Magnetic field studies at longer wavelengths

Magnetic fields can also be studied at radio wavelengths through their effect on the propagation of electromagnetic signals in plasma. We touch here of two of the main phenomena that are central to polarization studies at these wavelengths.

1.4.1 Synchrotron radiation

Given that radiation from charges arise from their acceleration, it is not surprising that electrons caught in and gyrating about magnetic field lines would emit polarized radiation. In the simplest case of **cyclotron radiation** from a single non-relativistic electron it can be shown the radiated electric field measured by a stationary observer located at a distance r in the far-field in the direction $\mathbf{n}$

$$\mathbf{E}_{\rm rad} \;=\; \frac{1}{cr^2}\left[\mathbf{n}\times\left(\mathbf{n}\times\frac{\partial^2\mathbf{p}_{\rm ret}}{\partial t^2}\right)\right] \tag{1.58}$$

will exhibit circular and/or linear polarization components depending on the orientation of the unit vector $\mathbf{n}$ relative to the electron's electric dipole moment component $\mathbf{p}_{\rm ret}$ in the plane perpendicular to the magnetic induction field $\mathbf{B}$ (and evaluated at the retarded time $t' = t - r/c$; note that Gaussian units are used in equation 1.58 and all others in this section). Such calculations reveal that the spectrum of cyclotron radiation is simple in that it contains only the frequency of gyration

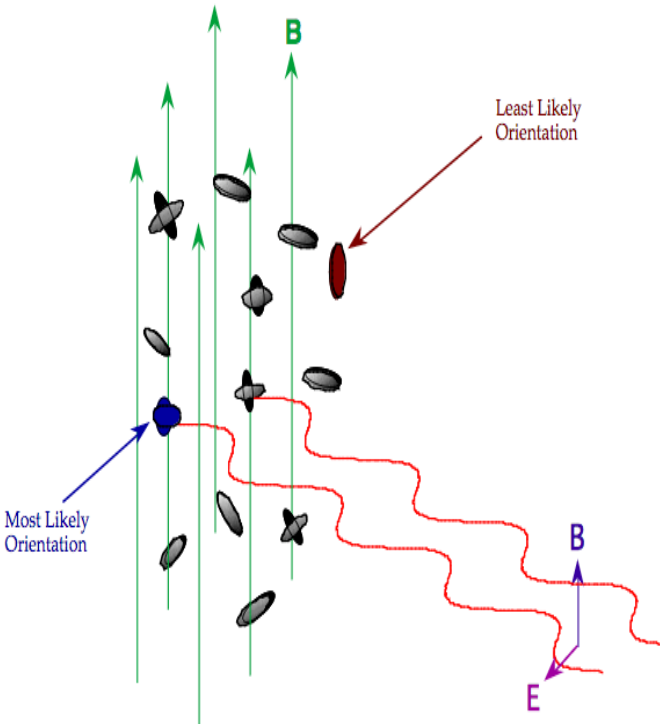

Figure 1.14: Cartoon showing the polarization of light emitted from dust grains. Because they emit more efficiently photons that are polarized along their long axis, the resulting electric field will be partially polarized in that orientation. The polarized signal is aligned perpendicularly relative to the plane of the sky component of the magnetic field.

$$\omega_{\rm g} = \frac{qB}{mc}. \tag{1.59}$$

Exercise 1.3. Single-charge cyclotron. Consider a charge q of mass m immersed in a region harbouring a uniform magnetic induction field $\mathbf{B} = B\mathbf{e}_z$, while at the same time being subjected to an arbitrary, and also uniform, force $\mathbf{F} = F\mathbf{e}_\perp$, where the unit vector $\mathbf{e}_\perp$ is located in the plane perpendicular to $\mathbf{e}_z$. Focus solely on the motion of the particle in that perpendicular plane and define the velocity of the particle as

$$\mathbf{u}_\perp \equiv \mathbf{u}_{\rm d} + \mathbf{u}_{\rm g}, \tag{1.60}$$

where $\mathbf{u}_{\rm g}$ is due to the expected gyrating (i.e., circular) motion of the charge about the magnetic field lines. We therefore expect that $u_g \propto e^{\pm i\omega_{\rm g} t}$ and write $\langle \mathbf{u}_{\rm g} \rangle = 0$ and $\mathbf{u}_{\rm d} = \langle \mathbf{u}_\perp \rangle$. That is, the **drift** velocity is the mean value of the total velocity of the particle and we further assume that it is constant.

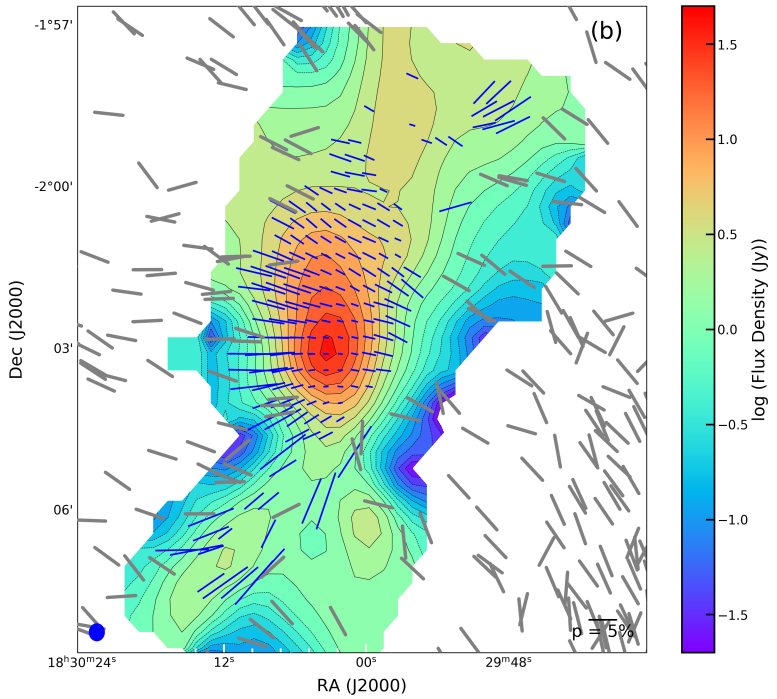

Figure 1.15: Polarimetry map of Serpens South from SOFIA/HAWC+ at 214 μm (emission; blue vectors) and with SIRPOL in the near-infrared (H band) (differential absorption; grey vectors). Both sets of vectors show the orientation of the magnetic field on the plane of the sky. From Pillai et al. 2020, Nat. Ast., 4, 1195.

Show that the gyration frequency is given by equation (1.59) and the radiated electric field scales as

$$\mathbf{E}_{\rm rad} \propto -qr_{\rm g}\omega_{\rm g}^2 \left[\cos\left(\omega_{\rm g}t'\right)\mathbf{e}_x \pm \sin\left(\omega_{\rm g}t'\right)\mathbf{e}_y\right] \tag{1.61}$$

when $\mathbf{n} = \mathbf{e}_z$ with $r_{\rm g}$ the gyration radius and where the '$\pm$' sign depends on the sense of gyration of the charge, while it is

$$\mathbf{E}_{\rm rad} \propto -qr_{\rm g}\omega_{\rm g}^2 \sin\left(\omega_{\rm g}t'\right)\mathbf{e}_y \tag{1.62}$$

when $\mathbf{n} = \mathbf{e}_x$.

The analysis is more complicated when the electron is moving at a relativistic velocity $\mathbf{u} = \boldsymbol{\beta}c$. In this case, an analysis similar to that of Exercise 1.3 shows that the frequency of gyration is replaced by the **synchrotron frequency**

$$\omega_{\rm s} = \frac{qB}{\gamma mc} \tag{1.63}$$

with $\gamma = \left(1-\beta^2\right)^{-1/2}$, while the radiation resulting from the acceleration of the charge results from the far-field electric field

$$\mathbf{E}_{\rm rad} = \frac{q}{c}\left[\frac{\mathbf{n}\times\left\{(\mathbf{n}-\boldsymbol{\beta})\times\dot{\boldsymbol{\beta}}\right\}}{(1-\mathbf{n}\cdot\boldsymbol{\beta})^3\,R}\right]_{\rm ret} \tag{1.64}$$

measured by an observer (at rest) at the retarded time. Considering different orientations for $\mathbf{n}$ (as in Exercise 1.3) once again reveals the polarization state to be elliptical in general, but with a much more complex frequency spectrum than in the non-relativistic case where all harmonics ($n\omega_{\rm s}$, for $n = 1, 2, 3, \ldots$) of the fundamental synchrotron frequency are potentially present. This also leads to complicated waveforms for the electric field, while the corresponding irradiated power is found to be

$$P = \frac{2}{3} r_0^2 c\gamma^2 \beta_\perp^2 B^2 \tag{1.65}$$

with $r_0 = q^2/mc^2$ for the electron's classical radius.

The problem is further complicated by the fact that radiation from strongly relativistic particle whose acceleration is perpendicular to its velocity (as is the case here) is characterized by a strong beaming, which implies that the radiation reaching the observer will be confined to a narrow solid angle of "radius" $\sim 1/\gamma$. But thus complication also brings in a significant simplification on the observational front.

As it turns out, the circular polarization component arising in equation (1.64) can be shown to average out to zero when combining the beaming effect and the single-charge radiation for a reasonable population of gyrating particles covering a range of pitch angles α between the magnetic field $\mathbf{B}$ and their velocities $\boldsymbol{\beta}$. That is, and perhaps counter-intuitively, **the state of the measured polarization for synchrotron polarization is strictly linear and peroendicular to the magnetic field on the plane of the sky**. While the total power radiated is found to be

$$P(\omega) \simeq \frac{\sqrt{3}}{2\pi}\frac{q^3 B}{mc^2}\sin(\alpha)\, F\left(\frac{\omega}{\omega_{\rm c}}\right), \tag{1.66}$$

integration over frequency yields a level of linear polarization of approximately 75% for a population of particles of a given energy (or γ). The function $F(\omega/\omega_{\rm c})$ in equation (1.66) is defined as

$$F(x) = x\int_x^\infty K_{5/3}(z)\, dz \tag{1.67}$$

with $K_n(z)$ is the modified Bessel function of order n, $x = \omega/\omega_{\rm c}$ and

$$\omega_{\rm c} = \frac{3}{2}\gamma^3\omega_{\rm s}\sin(\alpha), \tag{1.68}$$

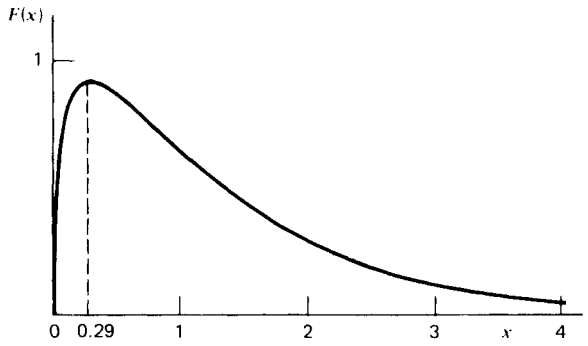

Figure 1.16: Functional form of $F(x)$, and thus of the total power $P(\omega)$, with $x = \omega/\omega_c$. Taken from Rybicki and Lightman (Chap. 6).

while its functional shape is shown in Figure 1.16.

1.4.2 Faraday rotation

The analysis of the propagation of radio waves through a plasma in a direction parallel to a uniform magnetic field $\mathbf{B}$ threading it reveals the presence of three distinct modes: one for *plasma oscillations* at the so-called *plasma frequency*

$$\omega_p = \sqrt{\frac{4\pi q^2 n}{m}} \tag{1.69}$$

with n the electron density, and two distinct modes for the propagation of circularly polarized plane waves with wave vectors

$$k_\pm = \frac{\omega}{c}\sqrt{1 - \frac{\omega_p^2}{\omega\left(\omega \mp \omega_g\right)}} \tag{1.70}$$

corresponding to the polarization states

$$\mathbf{e}_\pm = \frac{1}{\sqrt{2}}\left(\mathbf{e}_x \pm i\mathbf{e}_y\right) \tag{1.71}$$

when $\mathbf{B} = B\mathbf{e}_z$.

The difference between k_+ and k_- implies a birefringence of the medium since the corresponding group velocities $v_\pm = d\omega/dk_\pm$. It therefore follows that an incident linearly polarized wave with an electric field

$$\mathbf{E}_i = E_0\left[\cos(\theta)\,\mathbf{e}_x + \sin(\theta)\,\mathbf{e}_y\right] e^{i(kz-\omega t)} \tag{1.72}$$

will have its polarization state rotated by an angle

$$\Delta\theta(\omega) = (k_- - k_+)\,\frac{\Delta z}{2} \tag{1.73}$$

after propagating over a distance Δz. Importantly, this **Faraday rotation** of the linear polarization state is a function of the frequency of the wave. It can also bring a depolarization of the signal at finite spatial resolution since it is expected to vary with position in the source.

Exercise 1.4. Express the electric field of equation (1.72) in the $\mathbf{e}_\pm$ basis and use equation (1.70) to show that it is transformed to

$$\begin{aligned} \mathbf{E}_f &\propto E_0 \left[e^{-i(\theta+2\Delta\theta)} \mathbf{e}_+ + e^{i\theta} \mathbf{e}_- \right] e^{i(kz-\omega t)} \\ &\propto E_0 \left[\cos(\theta + \Delta\theta)\, \mathbf{e}_x + \sin(\theta + \Delta\theta)\, \mathbf{e}_y \right] e^{i(kz-\omega t)} \end{aligned} \tag{1.74}$$

after propagating over a distance Δz in plasma threaded by a uniform magnetic field $\mathbf{B} = B\mathbf{e}_z$, with $\Delta\theta$ given by equation (1.73).

It is generally the case that $\omega_\mathrm{g}, \omega_\mathrm{p} \ll \omega$ such that we can approximate to second order

$$k_\pm \simeq \frac{\omega}{c}\left(1 - \frac{\omega_\mathrm{p}^2}{2\omega^2}\right) \tag{1.75}$$

$$\begin{aligned} v_\pm^{-1} &= \frac{dk_\pm}{d\omega} \\ &\simeq \frac{1}{c}\left(1 + \frac{\omega_\mathrm{p}^2}{2\omega^2}\right). \end{aligned} \tag{1.76}$$

The second of the relations can be used to calculate the frequency dispersion of the propagation time

$$\begin{aligned} \frac{dt_\mathrm{p}}{d\omega} &= \frac{d}{d\omega}\left(\int_0^{\Delta z} \frac{dz}{v_\pm}\right) \\ &\simeq -\frac{4\pi q^2}{mc\omega^3} \int_0^{\Delta z} n dz \end{aligned} \tag{1.77}$$

with the **dispersion measure** defined as

$$\mathrm{DM} \equiv \int_0^{\Delta z} n dz. \tag{1.78}$$

Likewise, approximating to the next (i.e., third) order informs us on the variation of the Faraday rotation as a function of the frequency with

$$\frac{d(\Delta\theta)}{d\omega} = \frac{d}{d\omega}\left[\frac{1}{2}\int_0^{\Delta z} (k_- - k_+)\, dz\right]$$

$$\begin{aligned}
&\simeq \frac{d}{d\omega}\left\{\frac{\omega}{2c}\int_0^{\Delta z}\left[\left(1-\frac{\omega_{\rm p}^2}{2\omega\left(\omega+\omega_{\rm g}\right)}\right)-\left(1-\frac{\omega_{\rm p}^2}{2\omega\left(\omega-\omega_{\rm g}\right)}\right)\right]\right\}dz \\
&\simeq \frac{d}{d\omega}\left(\frac{2\pi q^3}{m^2c^2\omega^2}\int_0^{\Delta z} nB\,dz\right) \\
&\simeq -\frac{4\pi q^3}{m^2c^2\omega^3}\int_0^{\Delta z} nB\,dz \qquad (1.79)
\end{aligned}$$

with the **rotation measure** given by

$$\mathrm{RM} \equiv \int_0^{\Delta z} nB\,dz. \qquad (1.80)$$

Equations (1.77) and (1.79) are extremely important for magnetic field studies since the observations of compact sources of radiation at radio frequencies, e.g., pulsars, over a wide enough range will allow the determination of both the dispersion and rotation measures by studying the delay in pulse arrivals and variation of the linear polarization as a function of frequency. Their ratio thus yields an estimate of the "mean" magnetic field strength along the line of sight to the source with

$$\langle B\rangle \simeq \frac{\mathrm{RM}}{\mathrm{DM}}. \qquad (1.81)$$

An example of a magnetic field study in M51 using measurements of linear polarization from synchrotron radiation at $\lambda 3\,\mathrm{cm}$ and $\lambda 6\,\mathrm{cm}$ is shown in Figure 1.17. The slight misalignments between the magnetic field pseudo-vectors is due to differential Faraday rotation between the two wavelengths.

1.5 Analysis of polarization maps

We have already established in Sec. 1.2.1 that the Zeeman effect can reveal magnetic field strengths (usually $B_{\rm los}$) through polarimetry studies of spectral lines, but we also saw that the other processes we have reviewed (i.e., the Goldreich-Kylafis effect and dust polarimetry) can only reveal the morphology of the plane of the sky component of magnetic fields. It was, however, shown first by L. Davis Jr. (1951, PhRev, 81, 890) and then by S. Chandrasekhar & E. Fermi (1953, ApJ, 118, 113) that such maps could potentially reveal the strength of magnetic fields with an analysis of the dispersion of polarization vectors. As long as a few assumptions and approximations are made...

The basic idea underlying the DCF-method consists of modelling the magnetic field with two components such that

$$\mathbf{B} = \mathbf{B}_0 + \mathbf{B}_t \qquad (1.82)$$

where $\mathbf{B}_0$ and $\mathbf{B}_t$ are the large-scale (or mean or ordered) and turbulent (or random) parts of the overall field. We then assume that

- The turbulent component is weak, i.e., $B_t \ll B_0$.

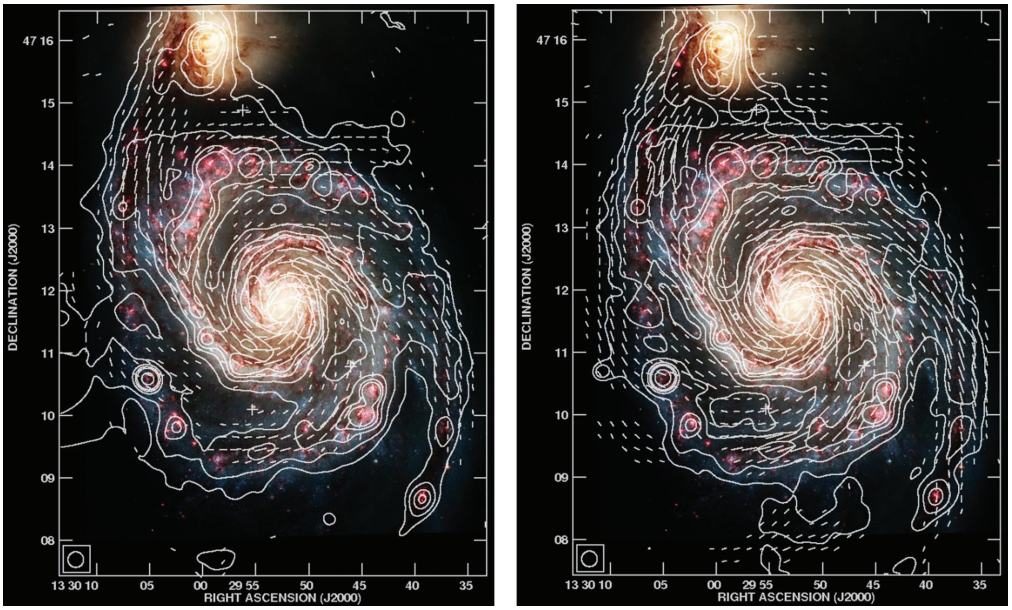

Figure 1.17: The orientation of the magnetic field in M51 as determined from measurements of linear polarization from synchrotron radiation at $\lambda 3\,\mathrm{cm}$ (left) and $\lambda 6\,\mathrm{cm}$ (right) obtained with the VLA and the Effelsberg observatory. The contours are for the total synchrotron intensity and the underlying optical image is from The Hubble Heritage Team. The slight misalignments between the magnetic field pseudo-vectors is due to differential Faraday rotation between the two wavelengths. The length of the pseudo-vectors scales with the polarized flux. Taken from Fletcher et al. 2011, 412, 2396.

- The turbulent component is zero-mean, i.e., $\langle \mathbf{B}_t \rangle = 0$.
- Deviations from the mean field are due to Alfvén waves, i.e., $\mathbf{B}_0 \cdot \mathbf{B}_t = 0$.
- And there is equipartition between turbulent kinetic and magnetic energies, i.e., $\rho v_t^2/2 = B_t^2/8\pi$.

This last equation is readily transformed to

$$v_t = \left(\frac{B_t}{B_0}\right)\left(\frac{B_0}{\sqrt{4\pi\rho}}\right), \tag{1.83}$$

and recognizing that the polarization angle $\Delta\theta = B_t/B_0$ we arrive at the DCF equation for the plane of the sky magnetic field strength

$$B_0 = \sqrt{4\pi\rho}\frac{v_t}{\Delta\theta}. \tag{1.84}$$

Starting with Davis and Chandrasekhar & Fermi and for many decades afterwards, estimates of magnetic field strengths were obtained with this equation by calculating a simple dispersion in the polarization angles (sometimes removing a large scale, ordered pattern, e.g., and hourglass) and using the line width from a suitable spectral line for v_t. It became clear early on that the technique had several shortcomings. For example, here are a few issues

- Turbulence in the ISM is not only due to Alvén waves (compressible modes exist).
- The mean field $\mathbf{B}_0$ must be fairly close to the plane of the sky.
- The assumption of weak turbulence (i.e., $\theta \ll 1$) is often violated.
- The measured signal is integrated along the line of sight and across the telescope beam, which artificially reduces the dispersion in $\Delta\theta$ (and overestimates B_0).

I show in Figure 1.18 a combination of the Zeeman $B_{\rm los}$ measurements of Fig. 1.7 and a compilation of published estimates of the plane of the sky magnetic field strength B_0 obtained with the DCF equation. It appears that the DCF method consistently overestimates the magnetic field strength.

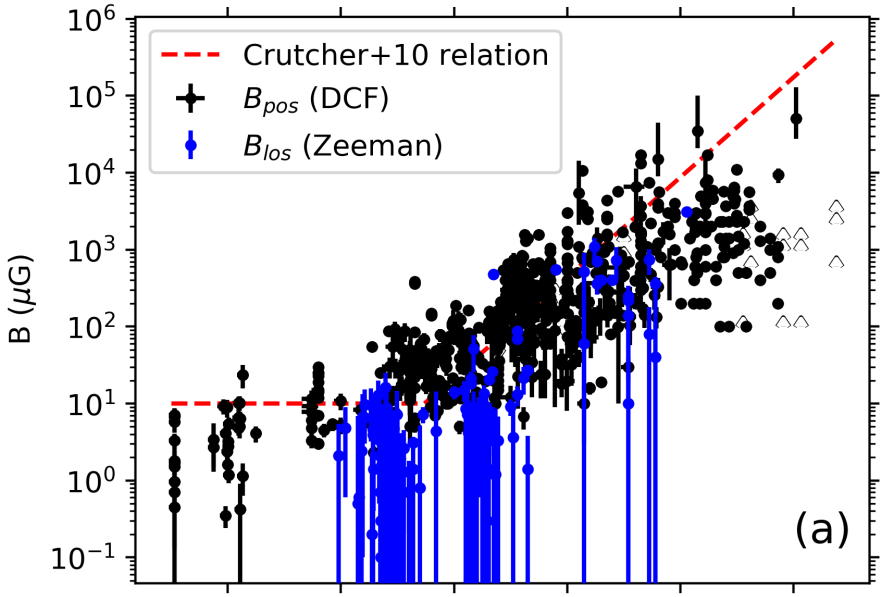

Figure 1.18: A combination of the Zeeman $B_{\rm los}$ measurements of Fig. 1.7 and a compilation of published estimates of the plane of the sky magnetic field strength B_0 obtained with the DCF equation. It appears that the DCF method consistently overestimates the magnetic field strength. From Pattle, Fissel & Tahani, 2022, arXiv:2203.11179v1).

Given these (and other) problems researchers spent a lot of time and efforts to improve the accuracy of the DCF method. MHD simulations were performed and led to modifications to equation (1.84), etc. I will end this lecture by discussing one approach that is now widely used to improve on estimates of magnetic field strengths.

1.5.1 Angular dispersion analysis of polarization maps

Improvements to the DCF method were realized when analysis techniques borrowed from turbulence studies were adopted. Namely, structure functions of the polarization angle came into play. There are several approaches and variations to this... my own preference is the following function that link changes between polarization angle at two points located a distance ℓ apart, $\Delta\theta(\ell) \equiv \theta(\mathbf{x}) - \theta(\mathbf{x}+\boldsymbol{\ell})$, and the magnetic field at the same points

$$\begin{aligned} \cos\left[\Delta\theta(\ell)\right] &= \frac{\mathbf{B}(\mathbf{x})\cdot\mathbf{B}(\mathbf{x}+\boldsymbol{\ell})}{\mathbf{B}(\mathbf{x})\cdot\mathbf{B}(\mathbf{x})} \\ &= \frac{\mathbf{B}\cdot\mathbf{B}(\ell)}{\mathbf{B}\cdot\mathbf{B}(0)}. \end{aligned} \tag{1.85}$$

Averaging this function over a polarization map for a given separation ℓ yields

$$1 - \langle\cos\left[\Delta\theta(\ell)\right]\rangle \simeq \frac{1}{2}\left\langle\Delta\theta(\ell)^2\right\rangle, \tag{1.86}$$

which is valid for small $\Delta\theta(\ell)$ (and thus small ℓ). The function within brackets on the right-hand side of equation (1.86) is the second order structure functions of the polarization angle.

With the assumption that the telescope beam and the autocorrelation function of the turbulence can be modelled by a Gaussian functions of widths W and δ, respectively, as well as other assumptions concerning the (joint) statistical properties of $\mathbf{B}_0$ and $\mathbf{B}_t$, it can be shown that equation (1.86) reduces to (Houde et al. 2009, ApJ, 706, 1504; 2016, ApJ, 820, 38)

$$1 - \langle\cos\left[\Delta\theta(\ell)\right]\rangle = \left[\frac{1}{1+N\left\langle B_0^2\right\rangle/\left\langle B_t^2\right\rangle}\right]\left[1 - e^{-\ell^2/2\left(\delta^2+2W^2\right)}\right] + \sum_{j=1}^{\infty} a_{2j}\ell^{2j}. \tag{1.87}$$

The last term on the right-hand side is a Taylor series representation for the contribution from the large scale (or mean) magnetic field, which can be readily fitted and removed from the data, while the other term is that due to turbulence. The quantity

$$N = \frac{\left(\delta^2+2W^2\right)\Delta'}{\sqrt{2\pi}\delta^3} \tag{1.88}$$

is the number of turbulence cells probed by the telescope beam. Since both the turbulence correlation length δ and the effective depth Δ' of the region under study can be

evaluated from the data (see below), N can be estimated and the aforementioned signal integration problem by can be addressed. Depending on the spatial resolution with which the polarization map was acquired, N can vary from 1 to several tens, i.e., the signal integration can sometimes be an important source of error and overestimation with the DCF equation.

An example of such a dispersion analysis for the CS ($J = 5 \rightarrow 4$) data is presented in Figure 1.19 for the CS ($J = 5 \rightarrow 4$) polarization map of Figure 1.10. The top panel shows the dispersion function (equation 1.86) as a function of the separation ℓ, and the broken curve is for the Taylor series fit to the large scale component (the $\sum_j a_{2j}\ell^{2j}$ term in equation 1.86), which is then removed to reveal the turbulence autocorrelation function $b^2(\ell)$ (bottom panel). This function is expressed by

$$b^2(\ell) = \left[\frac{1}{1 + N\left\langle B_0^2\right\rangle / \left\langle B_t^2\right\rangle}\right] e^{-\ell^2/2\left(\delta^2+2W^2\right)} \tag{1.89}$$

within the framework of our Gaussian model. In the bottom panel of Figure 1.19, the excess width of the autocorrelation function beyond that of the telescope beam (black broken curve) is a measure of the turbulence autocorrelation length, which was estimated to be $\delta \simeq 0.42$ arcsec or 2.6 mpc at the distance of NGC 6334 I(N) (1.3 kpc).

The value for the number turbulence cells found to be $N \simeq 1.4$ through equation (1.88) can be used with level at the peak of the autocorrelation function $b^2(0) \simeq 0.06$ to calculate the relative amount of turbulence in the magnetic field from

$$\begin{aligned} \frac{\left\langle B_t^2\right\rangle}{\left\langle B_0^2\right\rangle} &= N\left[\frac{b^2(0)}{1 - b^2(0)}\right] \\ &\equiv (\Delta\theta)^2 . \end{aligned} \tag{1.90}$$

The value thus calculated ($\left\langle B_t^2\right\rangle / \left\langle B_0^2\right\rangle \simeq 0.08$) is then inserted in the DCF equation with an average of the spectral line width ($v_t \simeq 5.3\,\mathrm{km\,s^{-1}}$) to get a plane of the sky magnetic field strength of $B_0 \simeq 2.8$ mG.

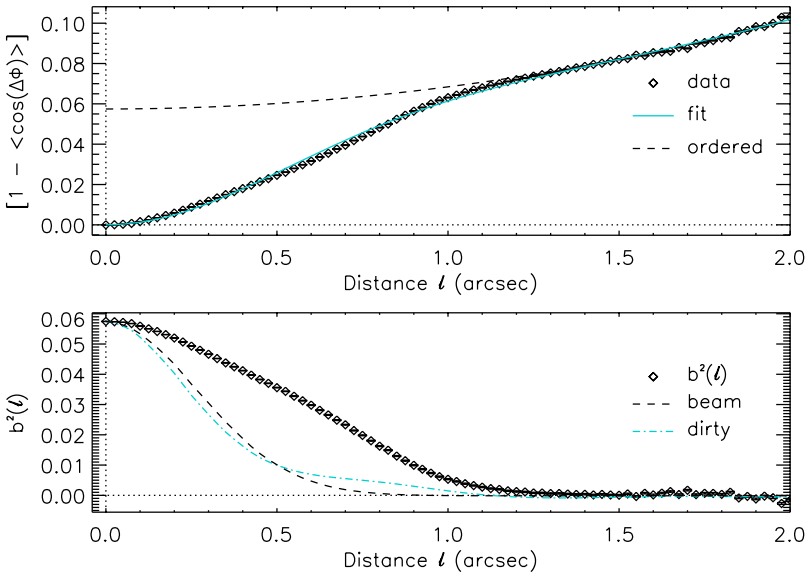

Figure 1.19: Dispersion analysis of the CS ($J = 5 \rightarrow 4$) polarization map presented in Figure 1.10. The top panel shows the dispersion function (equation 1.86) as a function of the separation ℓ. The broken curve is for the Taylor series fit to the large scale component, which is then removed to reveal the turbulence autocorrelation function $b^2(\ell)$ (bottom panel). In the bottom panel, the excess with of the autocorrelation function beyond that of the telescope beam is a measure of the turbulence autocorrelation length, which was estimated to be $\delta \simeq 0.42$ arcsec or 2.6 mpc at the distance of NGC 6334 I(N) (1.3 kpc).